ELSEVIER

Thin Solid Films 418 (2002) 163–168

thin solid films

www.elsevier.com/locate/tsf

X-Ray scattering study of crystallization behavior in homoepitaxial growth of $SrTiO_3$ films

Hsin-Yi Lee[a,*], Wei-Der Chang[a], C.-H. Hsu[a], K.S. Liang[a], J.Y. Lee[b], J.Y. Juang[b], K.H. Wu[b], T.M. Uen[b], Y.S. Gou[b]

[a]*Synchrotron Radiation Research Center, Hsinchu 30077, TaiwanROC*
[b]*Department of Electrophysics, National Chiao-Tung University, Hsinchu 30049, TaiwanROC*

Received 21 May 2001; received in revised form 16 February 2002; accepted 25 August 2002

Abstract

X-ray reflectivity and grazing incidence crystal truncation rod (CTR) measurements were employed to characterize the microstructure and crystallization behavior of homoepitaxial $SrTiO_3$ (STO) films deposited on polished $SrTiO_3$ (0 0 1) substrates by pulse laser deposition technique. X-ray scattering results indicate that room temperature grown STO film has a density approximately 11.1% lower than that of bulk STO and shows poor epitaxial relation with the substrate. Subsequent annealing at 760 °C for 20 s appeared to transform the film into two-layer structure, with the density of the layer right above the substrate approaching to its bulk value, while the density of the top 15.5 Å thick layer reducing to near 45% of bulk STO. The annealing process also leads to an increase of lateral lattice constant together with the growth of domain size. The appearance of interference fringes of the CTR after annealing, which is also observed at the film grown at 760 °C, clearly demonstrates the development of epitaxy upon short time annealing.

Keywords: X-Ray scattering; X-ray diffraction; Surfce structures; Growth Mechanism

1. Introduction

Since advanced electronic devices are continuing to shrink in size, ceramic capacitors and dynamic random access memories (DRAMs) require new and improved materials, which retain large dielectric properties at small dimensions. The demand of higher capacity and speed of computer system has driven scaling decrease of silicon integrated circuits. Conventional dielectric material used in IC industry, such as silicon dioxide (SiO_2) and silicon nitride (Si_3N_x) films are close to their application limit of thickness and dielectric strength. For film thickness down to a few nanometers, tunneling currents enhance the leakage current densities, thus reducing device reliability. This has promoted the study of high dielectric materials, such as TiO_2, Ta_2O_5, $Pb(Zr,Ti)O_3$, $SrTiO_3$, and $(Ba,Sr)TiO_3$, which permit an increase of the packing density of circuits without a further shrinkage of the insulator thickness. Among these, $SrTiO_3$, with a dielectric constant larger than 200, seems to be the most suitable and technology compatible candidate for metal-oxide-semiconductor devices and specifically for future generations of DRAMs [1,2].

Perovskite-type oxide thin films are very attractive materials due to their simple crystal structures and unique ferroelectric, dielectric, and optical properties. $SrTiO_3$ (STO) has been a hot research subject since 1960s. The crystal structure, dielectric properties, semiconductivity, even superconductivity have been extensively studied in wide temperature range [2–10]. The crystal structure of the STO unit cell is illustrated schematically in Fig. 1. However, the thin film technology for growing STO film has not yet been established.

*Corresponding author. Tel.: +886-3-5780281x7120; fax: +886-3-5789816.
E-mail address: hylee@srrc.gov.tw (H.-Y. Lee).

0040-6090/02/$ - see front matter
PII: S0040-6090(02)00770-8

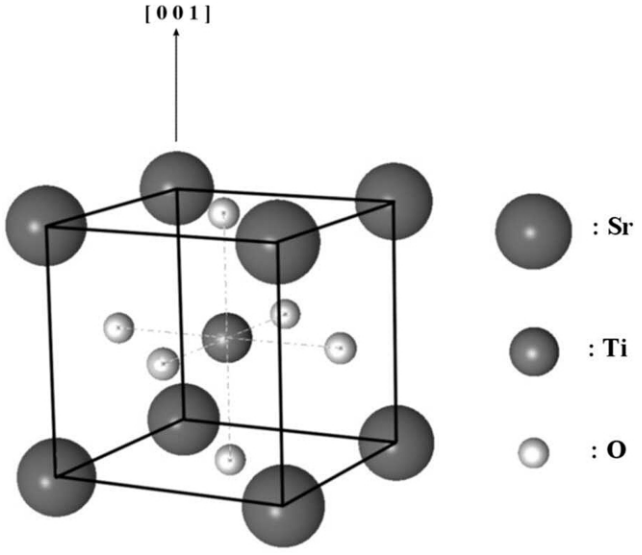

Fig. 1. Schematic diagram of the crystal structure of a STO unit cell.

Some reports [11,12] show that the properties of STO thin films grown under different conditions generally depart significantly from those of corresponding bulk materials, and annealing of STO films usually has improved the dielectric properties [2]. In our previous works, it was found that the growth mechanism of the homoepitaxial growth of STO films on stepped substrates is strongly dependent on the growth temperature and subsequent heat treatment [13,14]. Moreover, the detail information of the microstructure in thin films is of great importance because of its strong bearing on the properties and applications of STO films. Thus, understanding of the growth mechanism and the surface structure of a STO film on a microscopic scale is of significance for the fabrication of a new class of materials with artificially layered structure whose layer thickness and interface flatness are controlled on an atomic-scale. Therefore, a study of the microstructure and growth behavior of the STO films is thus interesting.

Whereas, X-ray diffraction (XRD) is one of the most ubiquitous techniques for structural characterization of crystalline phases, X-ray reflectivity has been demonstrated to be very powerful technique in studying the structure of the buried interface and the surface morphology. Below the critical incident angle, X-rays reflect totally from the solid surface in the same way as total optical reflection. When the incident angle increases above the critical angle, the reflected X-ray intensity falls rapidly. However, the interference among X-rays reflected from each interface gives an intensity modulation on the reflectivity curve, and, one is able to apply the X-ray reflectivity technique to characterize the film thickness, the interfacial roughness, and the electron density, etc. [15–20]. This nondestructive technique provides microscopic information about the roughness, density profile, and thickness of the layers that compose the thin film, and it offers advantages over ellipsometry in that precise information about the properties of buried layers can be obtained.

In recent years, there has also been growing interest in the application of grazing incidence X-ray technique for the study of the structure and morphology of buried layers and interfaces in thin films. Grazing-incidence XRD is a valuable analytical tool for the characterization of thin epitaxial films. To observe atomic-scale changes in surface morphology of thin epitaxial films, we can measure the features of crystal truncation rod (CTR) in the X-ray scattering pattern. The CTR pattern can be used to obtain values of the lattice parameter strain, film thickness, and interface roughness [21,22]. The results are essential in present-day thin film technology, and are used in the development of methods of growth and in the interpretation of the properties of thin films. Therefore, a combination of X-ray reflectivity and grazing incidence scattering measurement should serve as a very powerful technique for a simultaneous understanding of the buried interface structure and the growth behavior of thin film. In this paper, we applied X-ray scattering technique to study the effect of temperature on the microstructure of homoepitaxial STO films grown at room temperature (RT) and 760 °C.

2. Experimental procedure

STO films were deposited on polished STO (0 0 1) substrates by pulsed laser deposition (PLD) system equipped with an in situ reflection high-energy electron diffraction (RHEED) facility. The STO (1 0 0) substrates used were obtained from Shinkosha of Japan. A KrF excimer laser with pulse duration of 30 ns operated primarily at a repetition rate of 1 Hz was used for deposition. The laser energy was estimated to be approximately 2 J/cm^2. The target used was single-crystal disk of STO. All the films were deposited and annealed at an oxygen pressure of 5×10^{-4} Torr. The substrate temperature during deposition or annealing was controlled at RT and 760 °C, respectively. A RHEED system was used for in situ monitoring of film growth. The energy of the electron beam used for in situ RHEED diagnostics was 20 keV with a grazing angle of 0.7°, and was directed along the [1 0 0] direction of the STO substrate. With a de Broglie wavelength of approximately 0.86 Å, the grazing electron beam is slightly off Bragg conditions. The intensity evolution of the specular reflection was obtained by transmitting the diffraction images recorded by a charged coupled device camera to a frame-grabber board. The image was digitized by a flash analog-to-digital converter and stored in the memory buffer for subsequent display and analyses.

Surface morphology of the films was examined by atomic force microscopy (AFM). The AFM image was

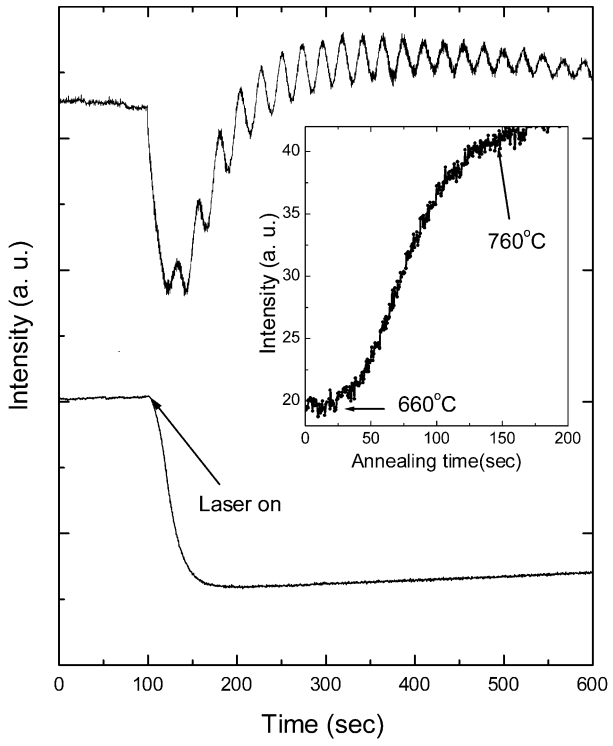

Fig. 2. The intensity oscillations in the RHEED patterns for STO films deposited at (a) RT; and (b) 760 °C. The inset plots show a dramatic jump in RHEED intensity for the RT film annealed at 760 °C.

taken by a Digital Instruments NanoScope II operated in air. The surfaces were scanned at different 2×2 μm^2 area with 3.052 Hz scan rate. The root-mean-square (RMS) of surface roughness was calculated automatically by a computer program. The thickness of the films was approximately 100 Å, as determined by X-ray reflectivity measurements.

The synchrotron X-ray scattering experiments were performed at wiggler beamline BL-17B at the Synchrotron Radiation Research Center (SRRC), Hsinchu, Taiwan. The electron storage ring was operated at energy of 1.5 GeV and current of 140–200 mA. The incident X-rays were focused vertically by a mirror and monochromatized to the energy of 8 keV by a Si (1 1 1) double-crystal monochromator. The sagital bend of the second crystal focused the X-rays in the horizontal direction. Using two pairs of slits between sample and detector, typical wave vector resolution in the vertical scattering plane was set to ~ 0.001 $Å^{-1}$ in this experiment.

3. Results and discussion

Fig. 2 shows the intensity oscillations in the RHEED pattern of STO films prepared under different conditions. The RHEED intensity exhibits an immediate damping with no oscillation when deposition takes place at RT (curve a). As the deposition temperature is raised to 760 °C, periodic oscillations in RHEED intensity appear immediately as the deposition starts (curve b). It infers that the growth mechanism of film is layer-by-layer [23]. When the RT film is annealed at 760 °C, a dramatic jump in RHEED intensity, as shown in the inset plot of Fig. 2, is detected after 20 s isothermal heating. The heating source is then turned off at this point for X-ray scattering study.

Fig. 3 displays the X-ray reflectivity curves of three different STO films deposited on STO substrate by PLD under different conditions. As compared to the sample deposited at high temperature (760 °C), the interference fringes of reflectivity curve of RT film exhibit prominent oscillations. Qualitatively, the fringes result from the interference among X-rays scattered by the electron density difference between substrate and film at the interface regime; the period of the fringes reflects the thickness of the films. This large oscillation amplitude refers to obvious difference of electron density between the thin layer and the substrate. The detailed profile near total reflection angle, illustrated in the inset of Fig. 3, confirms that the density of RT film is much lower than that of the films deposited (or annealed) at high temperatures which is slightly lower than that of STO substrate.

The principles of X-ray reflectivity were first reported by Parratt [15] in 1954 using the recursion formula for the reflectivity of a multi-layer system. In this work, we use the modified Parratt's recursive formalism to incor-

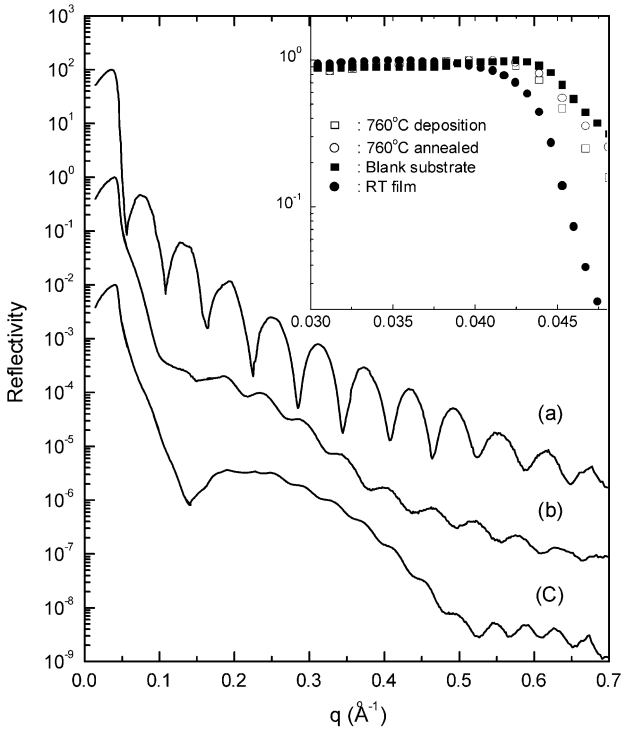

Fig. 3. X-Ray reflectivity curves of three different STO films for (a) RT film; (b) 760 °C annealed; and (c) 760 °C deposition. The inset plots illustrate the detailed profiles near total reflection angle.

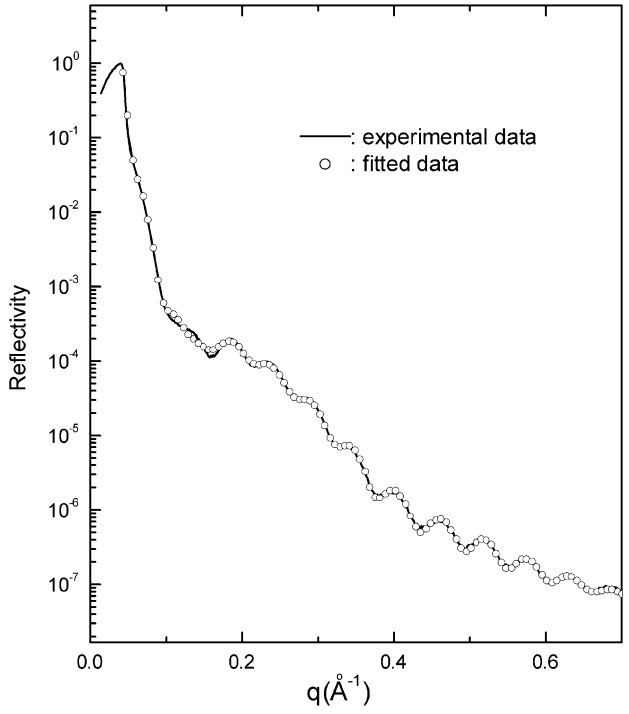

Fig. 4. X-Ray reflectivity curve and the corresponding best fit of a STO film deposited at RT and annealed at 760 °C for 20 s.

porate the effect of interface roughness. The detailed procedure was discussed by Lucas et al. [19]. The least square analysis was applied to obtain the best fitting result. The film is modeled as a sequence of layers of varying roughness, electron density, linear absorption coefficient, and the thickness. The instrumental resolution was estimated from the slit setting, and taken into account in the model calculation by convoluting a Gaussian function. The reflectivity curves of the samples prepared at high temperature deposition or deposited at RT then annealing at 760 °C for 20 s clearly exhibit oscillation of two different frequencies. The result suggests that the film has transformed into a structure consisted of more than one layers. Indeed, the fitted result indicates that, in addition to the originally deposited STO layer, an extra layer is existent in the deposited films.

Fig. 4 shows an experimental reflectivity curve (solid line) of a STO films deposited at RT then annealing at 760 °C for 20 s and its best-fitted data (open circle). The fitted curves match quite well with the experimental data even at a large momentum regime for all samples. It reveals that the proposed fitting model is proper for the present STO system. The values of each parameter obtained from the best-fitted results are summarized in Table 1. In comparison with the bare STO substrate, the best-fitted result of RT film shows an 11.1% loss of density. After 20 s annealing at 760 °C, the reflectivity curve of the RT sample shifts towards the film deposited at 760 °C, an indicative of density increase. However, the fitting result shows a three-layer model, including a thin top layer, a thick layer, and the STO substrate is needed to fit the measured reflectivity curves of the samples prepared at high temperature deposited and annealed sample. The fitting parameter reveals an unusually density profile for both samples. For annealed sample, the density of the thick layer with ~103 Å thick is 92.5% of STO substrate, but the density of the top layer, approximately 15.5 Å thick, is only approximately 45% of STO substrate. The best fitting result of the film deposited at 760 °C also shows a similar density configuration. The density of the thick layer, approximately 106 Å thick, is 97.8% of STO substrate, and the density of the top layer of 18.2 Å thick is approximately 43% of STO substrate. High temperature treatment indeed increases the density of the thick layer, but also significantly decreased the density of the top layers region in both samples. The density deviation at the top thin layer regions of fitted results obtained from the X-ray reflectivity measurement has also been confirmed by Secondary Ion Mass Spectrometry (SIMS) experiments. Fig. 5 shows the depth profiles of SIMS for three

Table 1
Parameters obtained from the best-fitted results of the reflectivity curves for STO films

Sample	Layer	Density	Thickness (Å)	Interface Roughness (Å)	AFM[a] Surface roughness (RMS; Å)
RT deposition	1	$(0.889\pm0.03)\ \rho$	116 ± 1	2.0 ± 0.1	1.6 ± 0.1
	2 (substrate)	∞	∞	2.03 ± 0.1	
760 °C annealing	1	$(0.45\pm0.01)\ \rho$	15.5 ± 0.5	3.88 ± 0.2	3.2 ± 0.2
	2	$(0.925\pm0.03)\ \rho$	103 ± 1	2.84 ± 0.2	
	3 (substrate)	ρ	∞	2.01 ± 0.1	
760 °C deposition	1	$(0.43\pm0.01)\ \rho$	18.2 ± 0.5	2.67 ± 0.2	2.8 ± 0.1
	2	$(0.978\pm0.03)\ \rho$	106 ± 1	2.29 ± 0.2	
	3 (substrate)	ρ	∞	2.10 ± 0.1	

[a] For a direct comparison, the surface roughness values as obtained from AFM measurements were also included in this table. ρ is a theoretical STO substrate density = 5.118 g/cm^3.

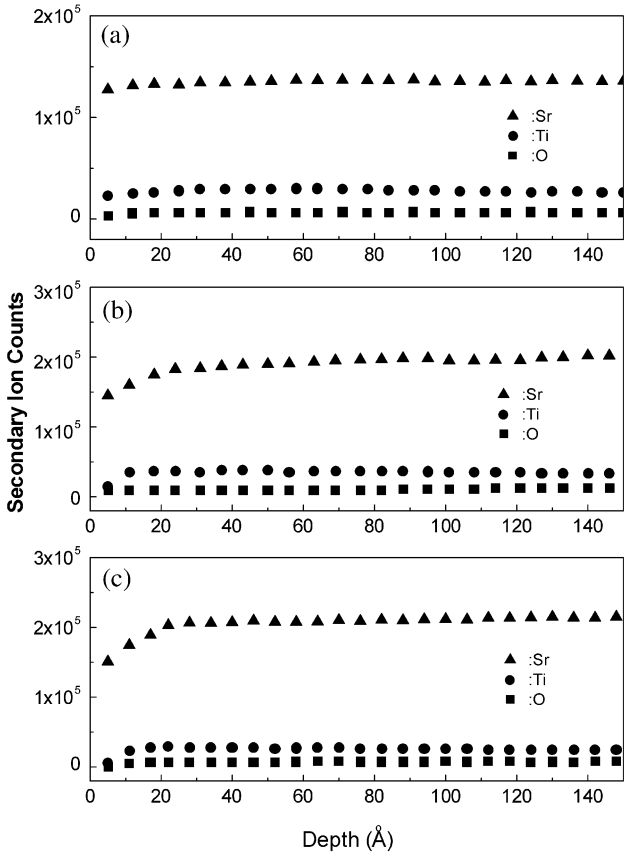

Fig. 5. Depth profile of SIMS of three different STO films for (a) RT film; (b) 760 °C annealed; and (c) 760 °C deposition.

different samples. It indicates that there is a reduced density of Ti and Sr atoms at top thin layer regions (~20 Å) for the film either deposited or annealed at 760 °C.

The surface morphology of a STO film deposited at high temperature as examined by AFM is shown in Fig. 6. The RMS surface roughness of the as-deposited STO surface layer is approximately 2.8 ± 0.1 Å. For the RT film, AFM measurement confirmed that the RMS roughness of top surface is increased from 1.6 to 3.6 Å after annealing, larger than the value of film deposited at 760 °C, 2.8 Å. The best-fitted result of X-ray reflectivity profiles also shows the same trend. RMS roughness of the top surface layer of RT film obtained from X-ray reflectivity measurement is also increased from 2.0 to 3.88 Å after annealing, larger than the value of film deposited at 760 °C, 2.67 Å. For a direct comparison, the surface roughness values as obtained from AFM measurements were also included in Table 1. The value of the surface roughness obtained from AFM is also in good agreement with the fitted results of X-ray reflectivity measurement.

In attempt to find the detailed structure modification after annealing and high temperature deposition, an in-plane scan approximately (0 2 0) diffraction peak is also performed using grazing incidence technique. The grazing incidence angle was fixed at 0.2° with respect to the sample surface, which is below the critical angle of any thin film samples in this study. In-plane grazing-incidence XRD measurement of these films show that the coherent size of substrate, deduced from the width of the Bragg peak in the in-plane direction by using Scherrer's formula [24], is approximately 7800 Å; while the crystal size of RT film and annealed film are ~1000 and ~1300 Å, respectively.

In addition, grazing incident CTR measurements approximately (1 1 1) Bragg peak, as shown in Fig. 7, provides more structural information. For the RT film, the (1 1 1) reflection consists of a single, sharp peak caused by the long-range order of substrate. On the other hand, distinct satellite fringes are observed for the film either deposited or annealed at 760 °C indicating that well epitaxial relation with the substrate has been developed along (1 1 1) plane for both samples.

4. Summary

Based on the X-ray scattering results and the RHEED intensity oscillations, the crystallization behavior of homoepitaxial STO films grown by pulse laser ablation technique may be understood as following. For the RT film, an average crystal size of ~1000 Å was formed on substrate with poor crystallinity. After annealed at 760 °C for 20 s, accompanied by a steep increase in RHEED intensity, domain size and lattice constant along lateral direction become larger and epitaxial structure similar to that of film deposited at 760 °C is rapidly developed. This indicates that annealing process provides the thermal energy for domain growth, and epitaxy aligning with substrate is initiated at film–substrate interface. Apparently, 20 s is inadequate for driving the

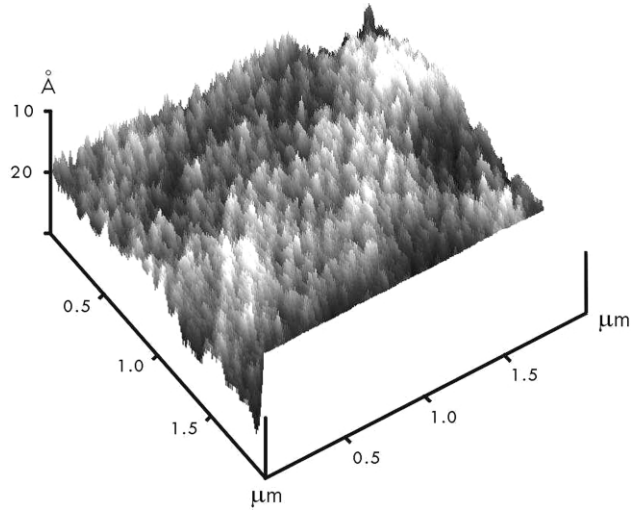

Fig. 6. A 3D AFM image of a STO film deposited at high temperature.

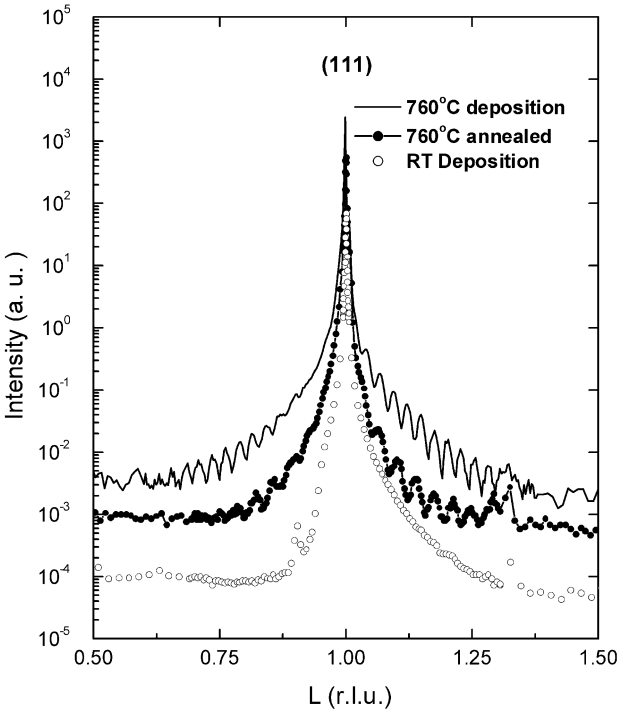

Fig. 7. Grazing incidence CTR measurements of three different STO films approximately (1 1 1) Bragg peak.

whole RT film to form the same epitaxial structure as the film deposited at 760 °C. From this, we speculate that the initial RT deposited film is already reasonable well align with the substrate although it has poor crystallinity. However, our results clearly demonstrate the structure transition of quasi-epitaxy thin films. In order to understand the details of structure re-orientation during the whole annealing period, a real-time X-ray scattering experiment will be carried out for further study.

Acknowledgments

This research was supported by the National Science Council of the Republic of China under the Contract No. NSC89-2216-E-213-001 and NSC88-2112-M009-020 (at National Chiao-Tung University).

References

[1] Y. Abe, M. Kawamura, K. Sasaki, Jpn J. Appl. Phys. 36 (Part 1) (1998) 5175.
[2] L. Ryen, X. Wang, U. Helmersson, E. Olsson, J. Appl. Phys. 85 (1999) 2828.
[3] G. Shirane, Y. Yamada, Phys. Rev. 177 (1969) 858.
[4] K.B. Lyons, P.A. Fleury, Solid State Commun. 23 (1977) 477.
[5] R.C. Neville, B. Hoeneisen, C.A. Mead, J. Appl. Phys. 43 (1972) 2124.
[6] G. Bednorz, K.A. Müller, Phys. Rev. Lett. 52 (1984) 2289.
[7] R. Viana, P. Lunkenheimer, J. Hemberger, R. Bühmer, A. Loidl, Phys. Rev. B 50 (1994) 601.
[8] H.P.R. Frederikse, W.R. Thurber, W.R. Holser, Phys. Rev. 134 (1964) A442.
[9] J.E. Schooley, W.R. Holser, M.L. Cohen, Phys. Rev. Lett. 12 (1964) 474.
[10] H. Suzuki, H. Bando, Y. Otuka, I.H. Inoue, J. Phys. Soc. Jpn 65 (1996) L1529.
[11] H. Tabata, H. Tanaka, T. Kawai, Appl. Phys. Lett. 65 (1994) 1970.
[12] S. Guo, H. Arwin, S.N. Jacobsen, K. Järrendahl, U. Helmersson, J. Appl. Phys. 77 (1995) 5369.
[13] J.Y. Lee, J.Y. Juang, K.H. Wu, T.M. Uen, Y.S. Gou, Surf. Sci. Lett. 449 (1–3) (2000) L235.
[14] J.Y. Juang, J.Y. Lee, Y.F. Chen, K.H. Wu, T.M. Uen, Y.S. Gou, Physica B 284–288 (1–4) (2000) 2099.
[15] L.G. Parratt, Phys. Rev. 95 (1954) 359.
[16] S.K. Sinha, E.B. Sirota, S. Garoff, H.B. Stanley, Phys. Rev. B 38 (1988) 2297.
[17] R.A. Cowley, T.W. Ryan, J. Phys. D 20 (1987) 61.
[18] S.M. Heald, H. Chen, J.M. Tranquada, Phys. Rev. B 38 (1988) 1016.
[19] C.A. Lucas, P.D. Hatton, S. Bates, W. Ryan, S. Miles, B.K. Tanner, J. Appl. Phys. 63 (1988) 1936.
[20] I.M. Tidswell, B.M. Ocko, P.S. Pershan, S.R. Wasserman, G.M. Whitesides, J.D. Axe, Phys. Rev. B 41 (1990) 1111.
[21] I.K. Robinson, Phys. Rev. B 33 (1986) 3830.
[22] I.K. Robinson, D.J. Tweet, Rep. Prog. Phys. 55 (1992) 599.
[23] T. Frey, C.C. Chi, C.C. Tsuei, T. Shaw, F. Bozso, Phys. Rev. B 49 (1994) 3483.
[24] B.E. Warren, X-Ray Diffraction, Dover, New York, 1990, p. 253.